APPLICATIONS OF 2D FULL WAVEFORM INVERSION TO RECORDED SHALLOW SEISMIC RAYLEIGH WAVES

M. Schäfer, L. Groos, T. Forbriger, and T. Bohlen

email: *M.Schaefer@kit.edu*

keywords: *Rayleigh waves, full-waveform inversion, field data application*

ABSTRACT

Shallow seismic Rayleigh waves can be excited by hammer blows on the surface and have high sensitivity to the S-wave velocity in the first meters of the subsurface. Therefore, they are attractive for geotechnical site investigations. Established methods for the inversion of surface waves are limited to 1D subsurface structures where the material properties vary only with depth. However, this assumption is not satisfied in many applications of practical relevance. To overcome this limitation we work towards a full waveform inversion (FWI) of shallow seismic Rayleigh waves. We present two field datasets which we acquired to test our 2D FWI approach. The first data example is recorded on a predominantly depth dependent structure while the second data example shows also lateral variations along the profile. Before applying FWI to field data we identified three essential preprocessing steps: 3D/2D transformation, consideration of anelastic damping and estimation of unknown source wavelets. We successfully applied our FWI strategy to the 1D field dataset. The resulting 2D S-wave velocity model is again predominantly depth dependent. We have also started applying FWI to the 2D field dataset. In this more complex case we identified further problems. Currently the inversion gets stuck in a local minimum.

INTRODUCTION

The inversion of shallow seismic surface waves is very attractive for geotechnical site investigations. Surface waves which are easily excited by a hammer blow have a high sensitivity to the shear wave velocity in the first meters of the subsurface. There are established methods to invert surface waves e. g. inversion of dispersion curves (Wathelet et al., 2004) or wavefield spectra (Forbriger, 2003). But all these methods assume 1D subsurface structures because they require consistent phase velocities along the profile. This assumption is not valid in many applications of practical relevance. To overcome this limitation we want to apply an elastic full waveform inversion (FWI) to shallow seismic surface waves. Previous applications have shown the high potential of this method (Romdhane et al., 2011; Tran and McVay, 2012; Bretaudeau et al., 2013). The application of a 3D FWI to surface waves unfortunately is still difficult due to excessive computational requirements. Therefore, we use a 2D inversion code originally developed by Köhn (2011). In the following we present data examples, essential preprocessing steps and inversion results.

DATA EXAMPLE I - 1D SUBSURFACE STRUCTURE

The first field dataset was acquired on a test site at Rheinstetten near Karlsruhe (Germany). The subsurface consists of layered fluviatile sediments. The acquisition geometry was a linear profile with 72 vertical geophones (eigenfrequency of 4.5 Hz) with an equidistant receiver spacing of 1 m. 25 shots were recorded along the profile where a vertical hammer blow was used as source.

DATA EXAMPLE II - 2D SUBSURFACE STRUCTURE

2D full waveform inversion is reasonably applicable to field data acquired on 2D structures. Scattering at 3D structures cannot be explained by 2D modelling. We selected a test site on the vertical fault system of the southern rim of the Taunus (near Frankfurt on the Main, Hesse, Germany). With preparatory investigations (seismics and DC geoelectrics) we confirmed the predominantly 2D nature of the subsurface. In the northwestern part of the vertical fault sericite-gneiss is met at shallow depth (0.5 - 2 m), while it is covered by sedimentary layers of up to 6 m thickness southeast of the fault. This is confirmed by Dynamic Probing Light (DPL) investigations and borehole profiles in the near vicinity. Perpendicular to this 2D fault we carried out a shallow seismic 2D survey in summer of 2011. We used 50 three component and 39 vertical component geophones (eigenfrequency of 4.5 Hz) and set up linear profiles of 89 m with 1 m receiver spacing. We employed 24 vertical hammer blows as vertical sources and we used an SH-source to excite horizontally polarized waves with horizontal hammer impacts. In Figure 1 a sketch of the survey layout and an exemplary shot in the southeast of the fault is plotted. We observe a significant change in the phase velocities along the profile which indicates significant lateral variations in the shallow subsurface. With additional seismic profiles parallel and one more perpendicular to the fault (dashed black lines in Figure 1a) we verified the 2D assumption.

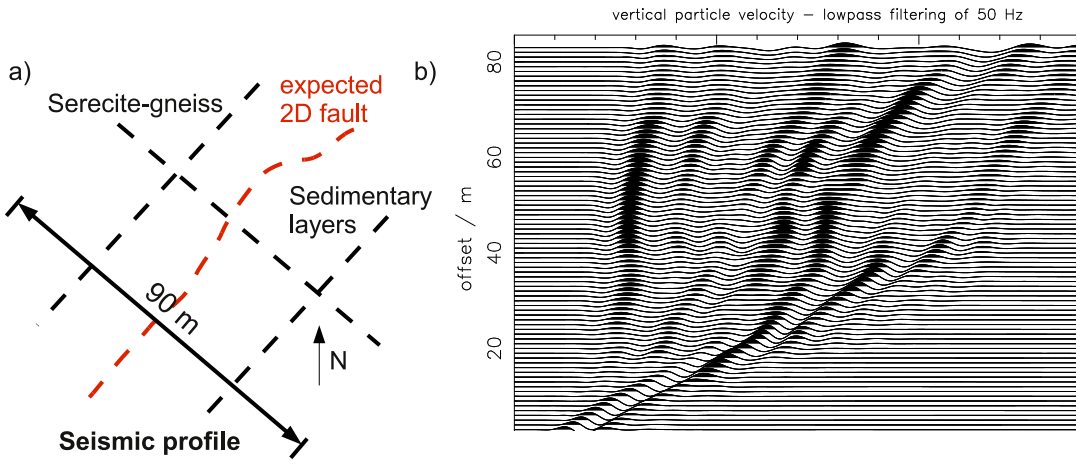

Figure 1: a) displays a sketch of the test site on a vertical fault system located on the southern rim of the Taunus (near Frankfurt on the Main, Hesse, Germany). The main seismic profile is displayed by the solid black line, additional seismic profiles which we used to verify the 2D assumption are displayed by the dashed black lines. The dashed red line indicates the location of the 2D fault. b) displays an exemplary common shot gather in the southeast of the fault of the main profile.

METHOD

We use a 2D elastic FWI code developed by Köhn (2011). It uses the time-domain adjoint method. The viscoelastic forward modelling is done with Finite Differences (FD) in the time domain (Bohlen, 2002). Viscoelastic damping is implemented by a generalized standard linear solid (Robertsson et al., 1994). We invert for elastic parameters (P-wave velocity, S-wave velocity and density) but not for parameters describing anelastic damping. As misfit definition we use the L2 norm of normalized wavefields where each trace is normalized by its RMS amplitude as suggested by Choi and Alkhalifah (2012). The misfit definition is not sensitive to an amplitude decay with offset. We apply frequency filtering during the inversion. We start with a bandwidth between 5 Hz and 10 Hz and increase the bandwidth sequentially during the inversion to higher frequencies. The gradients are preconditioned by semicircular windows around the source positions. The gradients and in some tests also the models are smoothed by 2D median filters. The filter lengths are always smaller than the minimum wavelength.

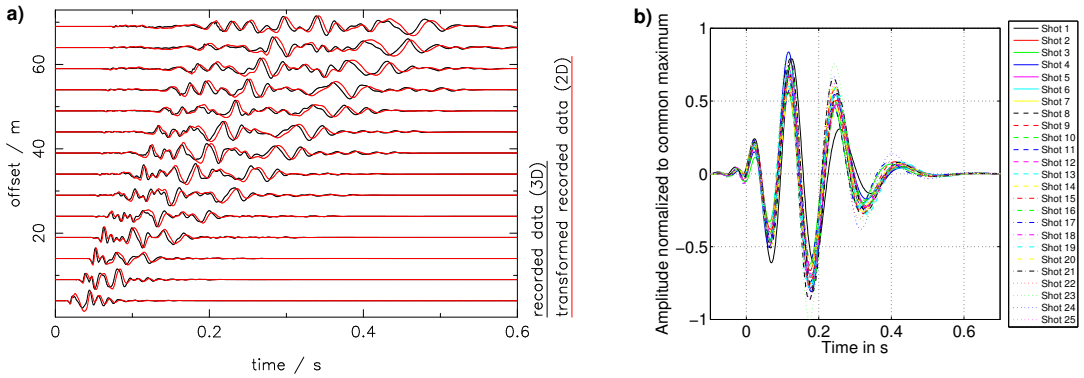

Figure 2: Preprocessing of field data acquired on the 1D subsurface structure. a) displays a comparison of recorded vertical velocity seismograms excited by a point source (black) and the corresponding estimated line source seismograms obtained by a 3D/2D transformation (red). Each trace is normalized to its maximum amplitude. b) displays estimated source wavelets for a bandwidth between 5 Hz and 10 Hz.

PREPROCESSING OF FIELD DATA

To apply 2D FWI to a field dataset acquired with point sources a geometrical spreading correction must be applied. Our 3D/2D transformation is based on the acoustic wave equation but we have approved that it is also valid in the elastic case by synthetic tests. The seismograms are convolved with $1/\sqrt{t}$. Afterwards they are tapered by $1/\sqrt{t}$ and scaled by the offset multiplied with $\sqrt{2}$ where t is the traveltime. Figure 2a displays a comparison of recorded seismograms and the corresponding transformed seismograms. The transformation produces a phase shift of $\pi/4$ as well as an amplitude scaling. The change in amplitude decay with offset is not observable due to the normalization of each trace.
From previous synthetic tests we know that anelastic damping cannot be neglected in an FWI of shallow seismic surface waves. Therefore, we use viscoelastic forward modelling with an a priori known quality factor in the FWI but do not invert for dissipative properties. For simplicity and to obtain physically consistent subsurface models we assume $Q_s = Q_p$ where Q_s is the quality factor of S-waves and Q_p of P-waves. To estimate the quality factor we simulate seismograms for different quality factors. For these simulations we use a subsurface model which describes the field data already as good as possible. The quality factor is then estimated by a comparison of the simulated data and the recorded data.
In an inversion of field data the unknown source wavelet for each shot must be estimated. We do this once at the beginning of each frequency bandwidth. The source wavelets are then used unaltered within this frequency band. The source wavelets are estimated by a stabilized deconvolution of the recorded data with the simulated data for the current subsurface model. Some exemplary source wavelets are displayed in Figure 2b.

RESULTS DATA EXAMPLE I

We applied the FWI to the field dataset acquired on the predominantly depth dependent structure. As initial P-wave velocity model we use the 1D model shown in Figure 3c which was gained from an analysis of first arrival P-wave travel times. As inital S-wave velocity model we use a 1D linear gradient (Figure 3d). In this test we only inverted for S-wave velocity and P-wave velocity. The density was kept unaltered during the inversion. As density model we use a model of a homogeneous layer (ρ=1700 $\mathrm{kg/m^3}$) over a homogeneous halfspace (ρ=2000 $\mathrm{kg/m^3}$) with a layer thickness of 6.8 m.

Figure 3e displays a comparison of seismograms for shot 25 at x=77 m. The data misfit is successfully decreased by FWI as the seismograms calculated with the final model fit the recorded data significantly better than the seismograms calculated with the initial model. Figure 3a-d displays the final 2D velocity models obtained by FWI. We observe 2D structures in the layer of the obtained P-wave velocity model. As the amplitude of the P-waves is much smaller compared to the Rayleigh waves the P-wave velocity model is not as well constrained as the S-wave velocity model and is therefore not further interpreted. The S-wave

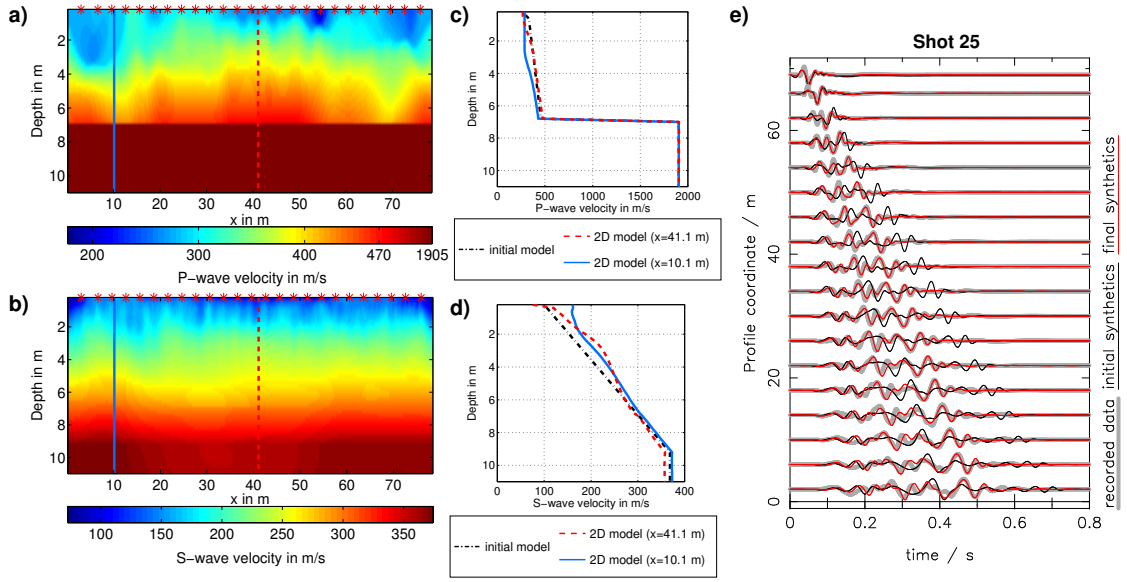

Figure 3: 2D subsurface model obtained by FWI applied to data example I. a) displays the P-wave velocity model and b) the S-wave velocity model. The red stars mark the source positions. Absorbing boundaries are cut off. c) and d) show the corresponding vertical velocity profiles in comparison to the initial model (dash-dotted black line). e) displays vertical displacement seismograms for shot 25 (x=77.0 m) in the frequency band between 5 Hz and 70 Hz. Recorded data are displayed by the thick grey line, seismograms calculated with the initial model are displayed in black and seismograms calculated with the 2D model are displayed in red. Each trace is normalized to its maximum amplitude.

velocity model still corresponds to a predominantly depth dependent structure. It seems that we cannot resolve structures that are deeper than 6.0 m. First tests indicate that this could be improved by a better preconditioning of the gradients (e. g. using the inverse of main diagonal elements of the approximate Hessian matrix or an amplification of low frequencies). Although the changes in the S-wave velocity model are small (Figure 3d) these changes have a strong influence on the wavefields (see Figure 3e) which confirms the high sensitivity of the Rayleigh waves to the S-wave velocity model. This makes FWI of shallow seismic Rayleigh waves interesting to image very shallow lateral inhomogeneities (e. g. filled ditches or sinkholes). More details on this application can be found in Groos et al. (2013).

RESULTS DATA EXAMPLE II - 10 HZ LOWPASS FILTERED DATA

To obtain a suitable starting model for the P-velocity model we have used a first arrival time tomography result. The P-velocity to density relation was taken from literature. The relationship of the P- and S-velocity is unknown to us but during synthetic tests we have gained good experience by using 1D linear gradients for the S-velocity model. The shallow S-velocity values are estimated from the phase velocity of the Rayleigh waves in the field dataset. The starting models of the FWI are plotted in Figure 4. The result of the travel time tomography for the P-velocity came as a surprise to us, because we expected a step like structure of the subsurface. But the tomography model fits the first arrivals of the field dataset very well.

We start the FWI with strongly lowpass filtered data at 10 Hz. Initially we need synthetic wavefields modelled on the current model (at the beginning the starting model) to obtain source wavelet correction filters for each single shot. This source wavelet will be updated when we increase the frequency content in the inversion. In Figure 5 (left side) the optimized source wavelets for the 10 Hz lowpass filtered data are shown. They are quite similar to each other and they have just a small acausal part which is a promising indication for an appropriate starting model. On the right side of Figure 5 the field data and the synthetics modelled on the starting and the final model are plotted. There is only a selection of representative traces of the near, middle and far field shown. In contrast to the full bandwidth we observe for the lowpass filtered

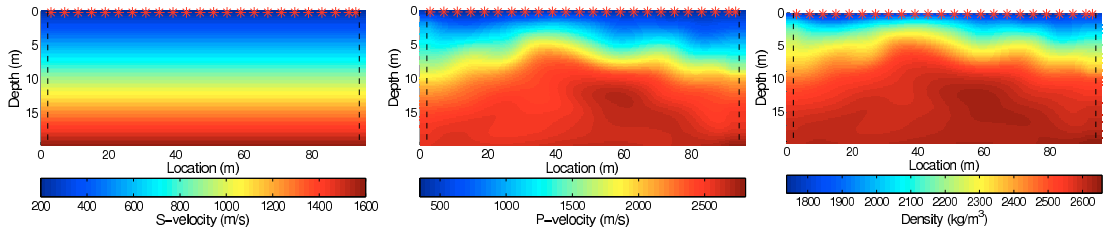

Figure 4: Starting models for the S-velocity, the P-velocity and the density of the FWI. Red stars denote the source locations and the dashed black line indicates the absorbing boundary used in the forward modelling.

data that almost the same phase velocities occur in the synthetics of the starting model and the field data. Hence, we have less problems with cycle skipping. When we apply the FWI we obtain a model for the S-velocity, the P-velocity and the density which produce synthetic wavefields that fit the field data in some features better. The fit of the near field traces is not much improved even in some parts it gets worse. In the offset range of 20 to 60 m we observe a very good fit of the synthetics of the final model and the field data. For the far field the fit becomes worse. The corresponding final S-velocity model is shown on the left side of Figure 6. We observe that the final model is smooth but there are some large-scale changes. This can be especially seen in the differences of the starting and the final model which are plotted on the right side in Figure 6. Here we can study the spatial changes in the model which indicate a 2D structure in the S-velocity model.

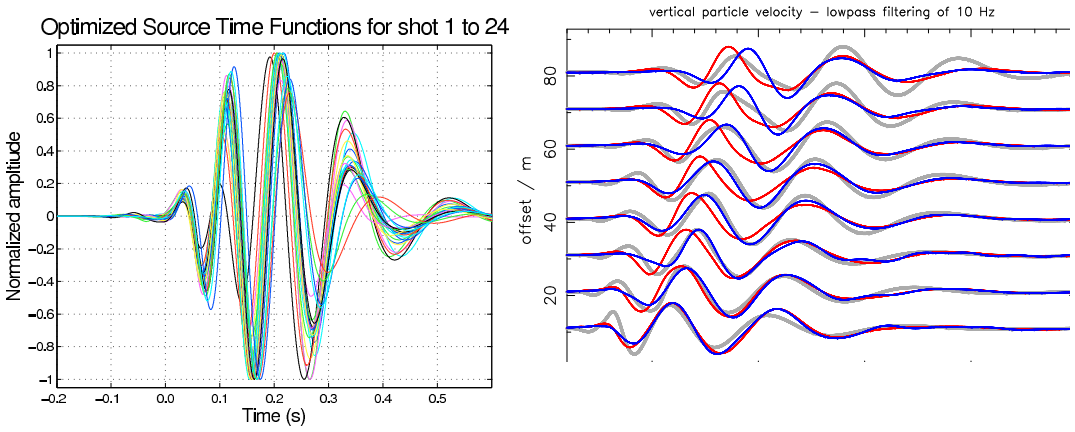

Figure 5: Optimized source time functions of the 10 Hz lowpass filtered data and comparison of recorded data with synthetics modelled on the starting and final model, respectively.

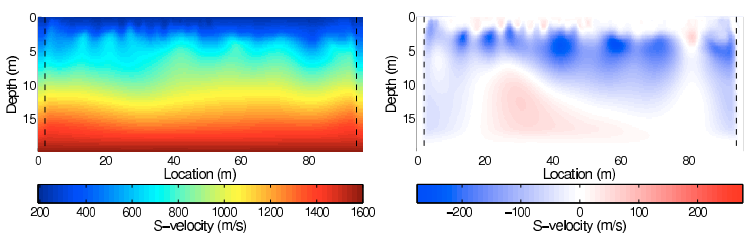

Figure 6: Preliminary S-velocity model and differences between the starting and the final model. Dashed black line indicates the absorbing boundary used in the forward modelling.

PROBLEMS WHEN ADDING HIGHER FREQUENCIES TO THE INVERSION

The inversion has to proceed with increasing bandwidth to infer smaller scale structure. But if we do so, we obtain strong local anomalies in the gradients (S-velocity, P-velocity and density). These anomalies are charaterized by 10^6 times larger values than their neighbors. The location of these anomalies isn't in the vicinity of source or receiver locations. It seems that the inversion is trapped in a local minimum. Recently we tried two different ways to tackle the problem. On the one hand we applied a preconditioning right on top of the anomaly to taper the artefact. This was only partially succesful, because it didn't improve the inversion result of higher frequencies. On the other hand we tried to implement a kind of regularisation to the inversion. The most simple regularisation is smoothing. We tested to correlate the filter length of the 2D median filter with the smallest present wavelength λ_{min} in the dataset. The filter length will be half the length of the smallest wavelength λ_{min}. E.g. for the 10 Hz lowpass filtered data the smallest wavelength is about $\lambda_{min} \approx 20$ m. Therefore, we use a 2D median filter with a filter length of 10 m to smooth the gradients. For higher frequencies the filter length is recalculated according to frequency content and seismic velocities. With this approach the anomalies occur no longer but the inversion fails for higher frequencies because no adjustment of the waveforms is observable.

Within these tests we kept the same starting model for the S-velocity. The approach of using 1D linear gradients for the S-velocity model worked for synthetic tests excellent but it maybe is not appropriate for field data application on 2D structure although the fit in Figure 5 for the starting model is quite reasonable. In a next step we will use a first arrival time tomography of SH-waves from the field data with the SH-source to obtain a more appropriate S-velocity model. A more detailed disussion is found in Schäfer et al. (2013).

SUMMARY

We present two field datasets which we acquired to test our 2D FWI approach. The first data example is recorded on a predominantly depth dependent structure while the second data example shows also lateral variations along the recorded profile. Before applying FWI to field data we have identified three essential preprocessing steps: 3D/2D transformation, consideration of anelastic damping and estimation of unknown source time functions of hammer impacts. We successfully applied our FWI strategy to the 1D field dataset. The resulting 2D S-wave velocity model is again predominantly depth dependent. Furthermore, we are currently working at the application of FWI to the 2D field dataset but in this more complex case we have to deal with further problems. At the moment it seems that the inversion is trapped in a local minimum. We tried different ways to overcome this problem like preconditioning and smoothing but could not find a proper solution yet. In a next step we want to improve the starting model of the S-velocity by a first arrival time tomography with SH-waves.

ACKNOWLEDGMENTS

This work was funded by the Federal Ministry of Education and Research grant 03G0752 (project TOAST). It was also kindly supported by the sponsors of the *Wave Inversion Technology (WIT) Consortium*, Germany. The 2D FWI code DENISE is available under the terms of GNU GPL at www.opentoast.de.

REFERENCES

Bohlen, T. (2002). Parallel 3-D viscoelastic finite difference seismic modelling. *Comput. Geosci.*, 28:887–899.

Bretaudeau, F., Brossier, R., Leparoux, D., Abraham, O., and Virieux, J. (2013). 2D elastic full-waveform imaging of the near-surface: application to synthetic and physical modelling data sets. *Near Surface Geophysics*.

Choi, Y. and Alkhalifah, T. (2012). Application of multi-source waveform inversion to marine streamer data using the global correlation norm. *Geophysical Prospecting*, 60:748–758.

Forbriger, T. (2003). Inversion of shallow-seismic wavefields: Part I and II. *Geophys. J. Int.*, 153(3):719–752.

Groos, L., Schäfer, M., Forbriger, T., and Bohlen, T. (2013). Comparison of 1D conventional and 2D full waveform inversion of recorded shallow seismic Rayleigh waves. In *Extended Abstracts, Near surface geoscience 2013*, page Mo S2a 06. EAGE.

Köhn, D. (2011). *Time domain 2D elastic full waveform tomography*. PhD thesis, Christian-Albrechts-Universität zu Kiel.

Robertsson, J. O. A., Blanch, J. O., and Symes, W. W. (1994). Viscoelastic finite-difference modeling. *Geophysics*, 59(9):1444–1456.

Romdhane, G., Grandjean, G., Brossier, R., Rejiba, F., Operto, S., and Virieux, J. (2011). Shallow-structure characterization by 2D elastic full-waveform inversion. *Geophysics*, 76(3):R81–R93.

Schäfer, M., Groos, L., Forbriger, T., and Bohlen, T. (2013). 2D full waveform inversion of recorded shallow seismic Rayleigh waves on a significantly 2D structure. In *Extended Abstracts, Near surface geoscience 2013*, page Mo S2a 07. EAGE.

Tran, K. T. and McVay, M. (2012). Site characterization using gauss-newton inversion of 2-D full seismic waveform in the time domain. *Soil Dyn. Earthq. Eng.*, 43:16–24.

Wathelet, M., Jongmans, D., and Ohrnberger, M. (2004). Surface-wave inversion using a direct search algorithm and its application to ambient vibration measurements. *Near Surface Geophysics*, 2(4):211–221.